Hindawi
Journal of Electrical and Computer Engineering
Volume 2022, Article ID 7054024, 13 pages
https://doi.org/10.1155/2022/7054024

*Research Article*

# Modeling and Performance Analysis of ECS-HTCARQ Protocol in Interference Scenario

**Yongqiang Zhou, Qihao Wang, Zhenggang Song, Suoping Li, and Nana Yang**

*School of Science, Lanzhou University of Technology, Lanzhou 730050, China*

Correspondence should be addressed to Yongqiang Zhou; zhoupaper@126.com

Received 26 April 2022; Revised 30 July 2022; Accepted 12 August 2022; Published 7 September 2022

Academic Editor: Gurvinder S. Virk



To extend the lifetime of energy-constrained wireless networks, this paper proposes a three-node model of the wireless-powered cooperative communication network (WPCCN). The model consists of an energy-constrained source node, an energy-sufficient relay node, and a destination node and considers two different cochannel interference (CCI) sources at the relay and destination nodes. To ensure the reliability of data transmission, we introduce the cooperative automatic retransmission request (CARQ) protocol, propose the energy-constrained source that harvests and cooperates automatic retransmission request (ECS-HTCARQ) protocol in interference scenario, derive a closed-form expression for the outage probability under Rayleigh fading channels, and establish a discrete-time Markov chain (DTMC) model to analyze the system throughput. The relationship between parameters such as the energy harvesting time allocation factor and energy harvesting efficiency on the outage probability and the system throughput is obtained. Numerical results show that the difference in system throughput is small as the increasing number of transmissions at a high signal-to-interference ratio (SIR), but there is a significant reduction in the outage probability. Finally, the optimal value of the energy harvesting time allocation factor is given under this model.

## 1. Introduction

In recent years, for energy-constrained wireless networks, replacing or charging batteries is costly and not easily achievable; besides, it is not an effective and sustainable approach, while energy harvesting (EH) has received much attention from researchers as a reliable and sustainable technology that can prolong the network lifetime [1–3]. EH technology collects energy in two primary ways: one is to use natural energy, including wind energy, solar energy, and water energy; the other is to adopt electromagnetic radiation, where wireless radio frequency energy harvesting (RFEH) technology is advantageous, because energy-constrained nodes through the RF signal radiated in the environment for energy harvesting and then harvested energy for information transmission. The authors in [4] studied the optimization of network delay, power allocation, and energy transfer in wireless sensor networks (WSNs) for EH. Literature [5] adopted RFEH technology in wireless body area networks (WBANs) and proposed an energy-efficient sleep scheduling algorithm with work-on-demand to prolong the network life. With the further development of antenna technology and EH technology, RFEH technology was widely adopted in WSNs, WBANs, and wireless charging systems (WCS) [4–6].

Wireless energy transfer is transferring energy to other devices in a wireless way. Two technologies are using RFEH for powering wireless network devices: one is simultaneous wireless information and power transfer (SWIPT) and the other is the wireless-powered communication network (WPCN). In [7, 8], addressing the trade-off between energy transfer and information transmission, the authors compared the rate-energy (RE) domain and outer boundaries of two EH receivers (i.e., time switching (TS) and power splitting (PS)) under the SWIPT network architecture and provided a solution for designing the best practical receiver. For the problem of optimal power allocation, literature [9–11] investigated the PS receiving mechanism of SWIPT

and gave solutions according to different allocation standards. To increase the transmission range in the heterogeneous network (HetNet) environment, literature [12] proposed a hybrid backscatter communication model suitable for WPCN and adopted the harvest-then-transmit (HTT) mechanism to study the throughput maximization problem under this model. In [13], for addressing the information transmission problem of secondary networks under cognitive WPCN, the authors proposed a novel hybrid HTT and backscatter communication. However, this does not apply to long-distance energy supply and data transmission. Literature [14] investigated a hybrid relay node (HRN) relay-assisted WPCN, adopted a harvest-then-cooperate (HTC) mechanism, and gave an optimization algorithm for the energy efficiency of the joint duration and power allocation problems in amplify-and-forward (AF) and decode-and-forward (DF) strategies. In this paper, we focus on studying the trade-off between energy transfer and information transmission under the WPCN structure, consider energy supply by an energy-sufficient relay node, adopt the HTC mechanism, and discuss the relationship between the impact of parameters such as the time allocation factor on outage probability and system throughput.

The cooperative communication (CC) technique used relay nodes for assisting the source node to transmit information to the destination node, which enhanced the performance of system outage probability, throughput, and energy efficiency [15–20]. In cooperative relay networks, AF and DF are two relay-forwarding strategies used frequently. AF strategy has lower complexity and is usually used in network environments with poor channel quality, while DF has higher complexity and is used for better channel quality [21, 22]. Thus, this paper adopts the DF relay-forwarding strategy in the high signal-to-interference ratio (SIR) environment. To further improve performances such as outage probability and throughput of the communication network, literature [23, 24] introduced the CARQ technology, which significantly improved the network performances compared to the traditional ARQ. In WSNs, [25] proposed a novel CARQ technology and established a discrete-time Markov chain (DTMC) model, which outperformed the traditional ARQ with an increasing number of transmissions at long-distance communication. In [26], the authors used the Go-Back-N ARQ (GBn-ARQ) technology to study the error control system for underwater wireless sensor networks and also analyzed the performance of throughput and delay under different system parameters. Inspired by the literature [14, 25], we consider introducing CARQ technology to establish a three-node model of the wireless-powered cooperative communication network (WPCCN), further improving the performance of the considered network.

Due to the limited spectrum of resources in nature, it was essential to consider interference factors [27, 28]. For wireless communication networks in the interference scenario, literature [27, 28] used DF and AF strategies to study their systems, respectively, which gave solutions to improve the reliability of data transmission in the interference scenario. Since the interfering transmitter affects the quality of received signals at the relay and destination nodes, literature [29] investigates the energy efficiency performance of SWIPT-enabled collaborative relay networks with the interfering transmitter. Discovering a model where the relay collects both the interference and the source node signal has a higher energy efficiency than a model where the relay harvests only the source node signal. In this paper, we consider the existence of cochannel interference (CCI) at the receptive nodes, introduce CARQ technology to improve the network system performance, and study the network performance under the WPCCN. Finally, the energy-constrained source that harvests and then cooperates automatic retransmission request (ECS-HTCARQ) protocol in the interference scenario is proposed, modeled, and analyzed.

The main contributions of this paper are summarized as follows.

(1) To be more actual, we consider that there are different CCI nodes at the received signal nodes, use the DF relay forwarding strategy, and adopt selection combining (SC) to perform signal merging at the destination node. Finally, a three-node model of WPCCN in the interference scenario is given.

(2) This paper adopts the HTC mechanism to harvest energy and then cooperative transmission. This model studies the problem of supplying energy from energy sufficient relay node to an energy-constrained source node, which has the advantage of a wider energy supply and transmission range compared with the nonrelay node, so it is more suitable for the medium and long-distance scenario.

(3) We establish the DTMC model of ECS-HTCARQ. Based on this model, we derive the closed-form expressions of the outage probability and system throughput, obtain the relationship of parameters such as the time allocation factor on the outage probability and system throughput, and give the optimal time allocation factor under different parameter settings.

The remainder of this paper is organized as follows: Section 2 shows the system model and transmission mechanism, Section 3 gives the closed-form expression for the outage probability, Section 4 analyzes the system throughput, Section 5 is the numerical simulation section, and Section 6 gives the future work and outlook.

## 2. System Model and Transmission Process

Aiming at the improvement problem of WPCCN performance in an interference scenario, the ECS-HTCARQ protocol under the interference scenario is proposed. The system model is shown in Figure 1. The model consists of an energy-constrained source node $S$, a destination node $D$, an energy-sufficient relay node $R$, and cochannel interference sources $I_1$ and $I_2$ near $R$ and $D$. Among them, the channel fading coefficient is expressed as $h_{xy} \sim CN(0, \sigma_{xy}^2)$, the channel gain $|h_{xy}|^2$ obeys an exponential distribution with mean $\sigma_{xy}^2$, and $x \in \{S, R\}$, $y \in \{S, R, D\}$.

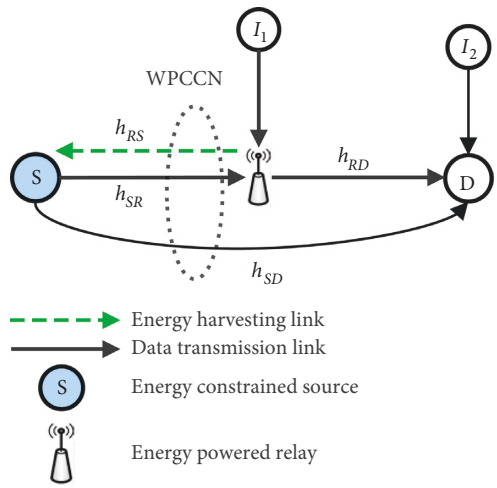


Figure 1: System model.

As shown in Figure 1, the system model consists of two parts: first, the energy-constrained source node $S$ harvests the RF signal broadcasted by the energy-sufficient relay node $R$; second, after the source node $S$ harvests end, the data transmission will take place. To improve the reliability of data transmission, the CARQ protocol with incremental redundancy is considered in this paper. The receiver has the memory of past data and accumulates mutual information for decoding data frames. During data transmission, the data packet is divided into multiple data frames, and when the data frame is received, $R$ and $D$ also receive the interference signal of $I_1$ and $I_2$, respectively. This paper sets that $S$ harvests energy each time which is only used for this data frame transmission, i.e., before $S$ transmits a data frame, which needs to harvest energy in advance (Note: This is determined by the energy storage space of the energy-constrained source node). Considering $D$ fails to decode but $R$ successfully decodes, when $S$ and $R$ retransmit the data frame, $R$ will forward the data frame in DF strategy and use SC for data merging at $D$; all nodes among the entire system work in half-duplex mode. In addition, let $T$ be the time from energy harvesting to the end of one frame data transmission, which is recorded as a data frame transmission process of the system (including energy harvesting and data frame transmission).

*2.1. Energy Harvesting (RF Signal).* Figure 2 shows the transmission process of the ECS-HTCARQ protocol. For the energy harvesting part, we adopt the HTC mechanism and introduce the time allocation factor $\alpha$. Within $\alpha T$ time, $S$ harvests the RF signal with energy from $R$, after the energy is collected, which is used for this transmission process.

*2.2. Data Frame Transmission Process.* As in Figure 2, $S$ performs data frame transmission within $(1-\alpha)T$. The transmission process of the ECS-HTCARQ protocol in the interference scenario is as follows: In this paper, we set the probability of $S$ successfully receiving the RF signal as 1. During the first stage $\alpha T$, $R$ broadcasts its RF signal carrying energy, which will be used for the next stage of data

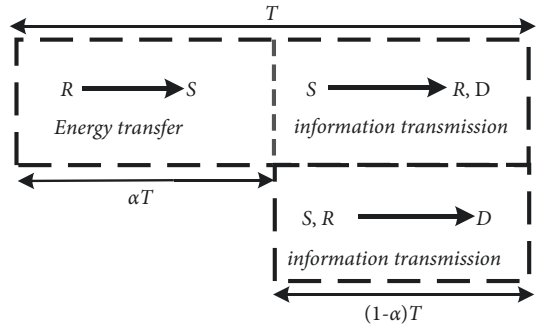


Figure 2: ECS-HTCARQ protocol transmission process in interference scenario.

transmission. In the second stage $(1-\alpha)T$, $S$ uses the energy harvested in the previous stage to broadcast the data frames to $R$ and $D$. The data frame transmission stages are divided into the following three situations:

(1) If $D$ successfully decodes the data frame from $S$, then $D$ will feedback an acknowledgment (ACK) to $S$. At this point, whether or not $R$ successfully decodes the data frame or not, $S$ will send a new data frame on the next transmission.

(2) Neither $R$ nor $D$ successfully decodes the data frame from $S$, then both feedback a negative acknowledgment (NACK) to $S$, and request $S$ to rebroadcast the data frame. If the maximum number of transmissions $L$ specified by the system has been reached but $D$ still fails to decode the data frame, the data frame will be discarded and $S$ will transmit a new data frame.

(3) If $R$ successfully decodes the data frame and $D$ fails to decode it, they will feedback ACK and NACK to $S$, respectively; then, $D$ will request $S$ to retransmit the decoded failed data frame. Since $R$ has successfully decoded the data frame in the previous transmission, $R$ will not receive the data frame in the retransmission, but $S$ and $R$ will send the data frame to $D$ at the same time. If $D$ fails to decode successfully after reaching the maximum transmission times $L$ specified by the system, the data frame will be discarded, and $S$ will transmit a new data frame.

In addition, we define $R_l$ as the successful decoding of a data frame from $S$ by $R$ at the $l$th time.

When $L = 3$ and $R_l = 2$, Figure 3 gives the successful transmission of one data frame for the ECS-HTCARQ protocol in the interference scenario.

## 3. Outage Probability Analysis

In this section, we calculate the outage probability of the ECS-HTCARQ protocol in the interference scenario. According to Figure 1, the receiver of an energy-constrained source node $S$ harvests energy from the RF signal that can be expressed as

$$E_S = \eta P_R \left|h_{R,S}\right|^2 \alpha T, \tag{1}$$

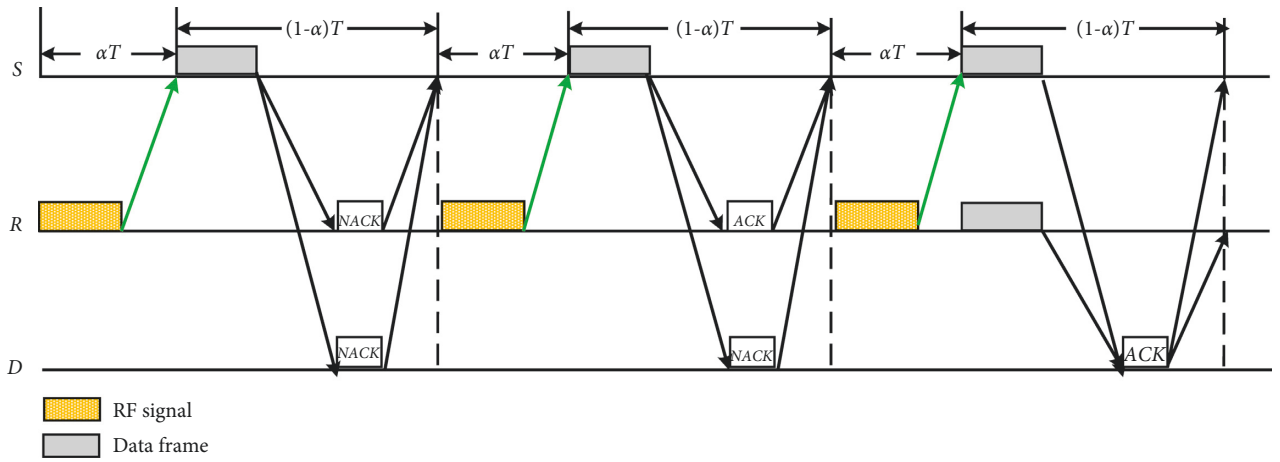


Figure 3: The successful transmission of one data frame for the ECS-HTCARQ protocol in the interference scenario.

where $0 < \eta < 1$ is the energy harvesting efficiency and $P_R$ is the transmit power of the relay node.

Since $S$ transmits the data frame within $(1-\alpha)T$, the transmit power of $S$ is

$$P_S = \frac{E_S}{(1-\alpha)T} = \frac{\alpha}{1-\alpha}\eta P_R |h_{R,S}|^2. \tag{2}$$

According to the system model, we consider the existence of interference sources during each transmission process and give expressions for the received signals of the $S-R$, $S-D$, $R-D$, and $S-R-D$ links, which are expressed by $Y_R$, $Y_{D_L}$, $Y_{D_R}$, and $Y_{D_{RL}}$, respectively:

$$\begin{aligned} Y_R &= \sqrt{P_S} h_{S,R} x_S + \sqrt{P_{I_1}} h_{I_1,R} x_1, \\ Y_{D_L} &= \sqrt{P_S} h_{S,D} x_S + \sqrt{P_{I_2}} h_{I_2,D} x_2, \\ Y_{D_R} &= \sqrt{P_R} h_{R,D} x_R + \sqrt{P_{I_2}} h_{I_2,D} x_2, \\ Y_{D_{RL}} &= \max\left(Y_{D_R}, Y_{D_L}\right), \end{aligned} \tag{3}$$

where source node $S$ and interference sources $I_1$ and $I_2$ that emit the normalized signals are $x_S$, $x_1$, and $x_2$, respectively.

We give the SIR received by the above four links in formulas (4)–(7):

$$\gamma_R = \frac{P_S |h_{S,R}|^2}{P_{I_1} |h_{I_1,R}|^2} = \frac{\alpha/1-\alpha\eta P_R |h_{R,S}|^2 |h_{S,R}|^2}{P_{I_1} |h_{I_1,R}|^2}, \tag{4}$$

$$\gamma_{D_L} = \frac{P_S |h_{S,D}|^2}{P_{I_2} |h_{I_2,D}|^2} = \frac{\alpha/1-\alpha\eta P_R |h_{R,S}|^2 |h_{S,D}|^2}{P_{I_2} |h_{I_2,D}|^2}, \tag{5}$$

$$\gamma_{D_R} = \frac{P_R |h_{R,D}|^2}{P_{I_2} |h_{I_2,D}|^2}, \tag{6}$$

$$\begin{aligned} \gamma_{D_{RL}} &= \max\left(\gamma_{D_R}, \gamma_{D_L}\right) \\ &= \max\left(\frac{P_R |h_{R,D}|^2}{P_{I_2} |h_{I_2,D}|^2}, \frac{\alpha/1-\alpha\eta P_R |h_{R,S}|^2 |h_{S,D}|^2}{P_{I_2} |h_{I_2,D}|^2}\right). \end{aligned} \tag{7}$$

We analyze the outage probability of the system under long-term static channels. In the long-term static channel, the channel fading coefficients are constant during each transmission and between frames are independent and identically distributed.

When an outage event occurs, the outage probability can be expressed as the transmission error probability of a data frame in a transmission. Assuming that the outage rate of the data link is $r$ bits/transmission time/Hz, the outage links can be indicated as

$$\Pr_{\text{out}} = \Pr\{\log(1+\gamma) < r\}. \tag{8}$$

In the $l$th transmission, $\Pr(SR_{\text{out},l})$, $\Pr(SD_{\text{out},l})$, $\Pr(SRD_{\text{out},l})$, and $\Pr(RD_{\text{out},l})$ are used to denote the outage probability of each link, and since the ARQ protocol with incremental redundancy is considered, we have

$$\Pr\left(SR_{\text{out},l}\right) = \Pr\left\{ l\log\left(1 + \frac{\alpha/1-\alpha\eta P_R |h_{R,S}|^2 |h_{S,R}|^2}{P_{I_1} |h_{I_1,R}|^2}\right) < r \right\}, \tag{9}$$

$$\Pr\left(SD_{\text{out},l}\right) = \Pr\left\{ l\log\left(1 + \frac{\alpha/1-\alpha\eta P_R |h_{R,S}|^2 |h_{S,D}|^2}{P_{I_2} |h_{I_2,D}|^2}\right) < r \right\}, \tag{10}$$

$$\begin{aligned} \Pr\left(SRD_{\text{out},l}\right) = \Pr\Bigg\{ & l\log\left(1 + \frac{\alpha/1-\alpha\eta P_R |h_{R,S}|^2 |h_{S,D}|^2}{P_{I_2} |h_{I_2,D}|^2}\right) \\ & < r, (l-R_l)\log\left(1 + \frac{P_R |h_{R,D}|^2}{P_{I_2} |h_{I_2,D}|^2}\right) < r \Bigg\}, \end{aligned} \tag{11}$$

$$\Pr\left(RD_{\text{out},l}\right) = \Pr\left\{ (l-R_l)\log\left(1 + \frac{P_R |h_{R,D}|^2}{P_{I_2} |h_{I_2,D}|^2}\right) < r \right\}. \tag{12}$$

In the appendix, we derive the closed-form expressions of equations (9)–(12), which can be expressed as equations (13)–(16):

$$\Pr\left(SR_{\text{out},l}\right) = 1 - \exp\left(\frac{\tau\sigma_{I_1,R}^2}{2\sigma_{R,S}^2\sigma_{S,R}^2}\right)W_{-1,\frac{1}{2}}\left(\frac{\tau\sigma_{I_1,R}^2}{\sigma_{R,S}^2\sigma_{S,R}^2}\right), \quad (13)$$

$$\Pr\left(SD_{\text{out},l}\right) = 1 - \exp\left(\frac{\tau_1\sigma_{I_2,D}^2}{2\sigma_{R,S}^2\sigma_{S,D}^2}\right)W_{-1,\frac{1}{2}}\left(\frac{\tau_1\sigma_{I_2,D}^2}{\sigma_{R,S}^2\sigma_{S,D}^2}\right), \quad (14)$$

$$\begin{aligned}\Pr\left(SRD_{\text{out},l}\right) &= 1 - \exp\left(\frac{\tau_1\sigma_{I_2,D}^2}{2\sigma_{R,S}^2\sigma_{S,D}^2}\right)W_{-1,\frac{1}{2}}\left(\frac{\tau_1\sigma_{I_2,D}^2}{\sigma_{R,S}^2\sigma_{S,D}^2}\right)\\ &\quad - \frac{\sigma_{R,D}^2}{\tau_2\sigma_{I_2,D}^2 + \sigma_{R,D}^2} + \exp\left(\frac{\tau_1\sigma_{I_2,D}^2\sigma_{R,D}^2}{2\sigma_{R,S}^2\sigma_{S,D}^2\left(\tau_2\sigma_{I_2,D}^2 + \sigma_{R,D}^2\right)}\right)\\ &\quad \times \frac{\sigma_{R,D}^2}{\tau_2\sigma_{I_2,D}^2 + \sigma_{R,D}^2}W_{-1,\frac{1}{2}}\left(\frac{\tau_1\sigma_{I_2,D}^2\sigma_{R,D}^2}{\sigma_{R,S}^2\sigma_{S,D}^2\left(\tau_2\sigma_{I_2,D}^2 + \sigma_{R,D}^2\right)}\right),\end{aligned} \quad (15)$$

$$\Pr\left(RD_{\text{out},l}\right) = 1 - \frac{\sigma_{R,D}^2}{\tau_2\sigma_{I_2,D}^2 + \sigma_{R,D}^2}. \quad (16)$$

## 4. System Throughput Analysis

Based on the transmission mechanism, we establish a DTMC model with $L(L+1)/2+1$ states under the condition that the maximum number of transmissions is $L$, as shown in Figure 4. As shown in Table 1, we give the meanings of states in the DTMC model. What needs to be pointed out is that we assume the relay can successfully decode the data frame in the next transmission once it decodes the data frame correctly in the $R_l$ transmission. In other words, the state $R_{i,j}$ can only shift to the state $R_{i+1,j+1}$, $A$ or $X$.

Based on the DTMC model, the one-step transition probabilities are yielded:

$$\begin{cases}
\Pr_{AA} = \Pr_{XA} = 1 - \Pr\left(SD_{\text{out},1}\right)\\
\Pr_{R_{i,j}A} = 1 - \Pr\left(SRD_{\text{out},i+1}|SRD_{\text{out},i}\right), 1 \le j \le i \le L-1, R_l = i - j + 1\\
\Pr_{E_iA} = 1 - \Pr\left(SD_{\text{out},i+1}|SD_{\text{out},i}\right), 1 \le i \le L-1\\
\Pr_{AE_1} = \Pr_{XE_1} = \Pr\left(SD_{\text{out},1}\right)\Pr\left(SR_{\text{out},1}\right)\\
\Pr_{AR_{1,1}} = \Pr_{XR_{1,1}} = \Pr\left(SD_{\text{out},1}\right)\left(1 - \Pr\left(SR_{\text{out},1}\right)\right)\\
\Pr_{E_iE_{i+1}} = \Pr\left(SD_{\text{out},i+1}|SD_{\text{out},i}\right)\Pr\left(SR_{\text{out},i+1}|SR_{\text{out},i}\right), 1 \le i \le L-2\\
\Pr_{E_iR_{i+1,1}} = \Pr\left(SD_{\text{out},i+1}|SD_{\text{out},i}\right)\left(1 - \Pr\left(SR_{\text{out},i+1}|SR_{\text{out},i}\right)\right), 1 \le i \le L-2, R_l = i+1\\
\Pr_{R_{i,j}R_{i+1,j+1}} = \Pr\left(SRD_{\text{out},i+1}|SRD_{\text{out},i}\right), 1 \le j \le i \le L-2, R_l = i - j + 1\\
\Pr_{R_{L-1,j}X} = \Pr\left(SRD_{\text{out},L}|SRD_{\text{out},L-1}\right), 1 \le j \le L-1, R_l = L - j\\
\Pr_{E_{L-1}X} = \Pr\left(SD_{\text{out},L}|SD_{\text{out},L-1}\right)
\end{cases} \quad (17)$$

We define the throughput as the average number of frames successfully decoded by the destination node $D$ in $(1-\alpha)T$, which can be computed as the average number of $(1-\alpha)T$ time that the DTMC spends in the state $A$, i.e., the product of the steady-state probability of state $A$ and the transmission time.

Assuming that both the first row and the first column of the one-step transition probability matrix of the DTMC model start from state $A$, the steady-state distribution of the model is $\pi = (\pi_1, \pi_2, \ldots, \pi_{L(L+1)/2+1})$, where $\pi_1$ is the steady-state probability of $D$ that decodes a data frame successfully. $\pi_1$ can be obtained from the following equilibrium equation and normalization condition:

$$\begin{cases}
\pi P = \pi\\
\sum_{i=1}^{L(L+1)/2+1} \pi_i = 1
\end{cases} \quad (18)$$

In particular, the system throughput is calculated for $L = 2$ and $L = 3$.

When $L = 2$, the one-step transition probability matrix $P$ of the DTMC model is given as

$$P = \begin{pmatrix}
\Pr_{AA} & 0 & \Pr_{AE_1} & \Pr_{AR_{1,1}}\\
\Pr_{XA} & 0 & \Pr_{XE_1} & \Pr_{XR_{1,1}}\\
\Pr_{E_1A} & \Pr_{E_1X} & 0 & 0\\
\Pr_{R_{1,1}A} & \Pr_{R_{1,1}X} & 0 & 0
\end{pmatrix}. \quad (19)$$

According to (18) and (19), we have

$$\begin{cases}
\Pr_{AA}\pi_1 + \Pr_{XA}\pi_2 + \Pr_{E_1A}\pi_3 + \Pr_{R_{1,1}A}\pi_4 = \pi_1\\
\Pr_{E_1X}\pi_3 + \Pr_{R_{1,1}X}\pi_4 = \pi_2\\
\Pr_{AE_1}\pi_1 + \Pr_{XE_1}\pi_2 = \pi_3\\
\Pr_{AR_{1,1}}\pi_1 + \Pr_{XR_{1,1}}\pi_2 = \pi_4\\
\pi_1 + \pi_2 + \pi_3 + \pi_4 = 1
\end{cases} \quad (20)$$

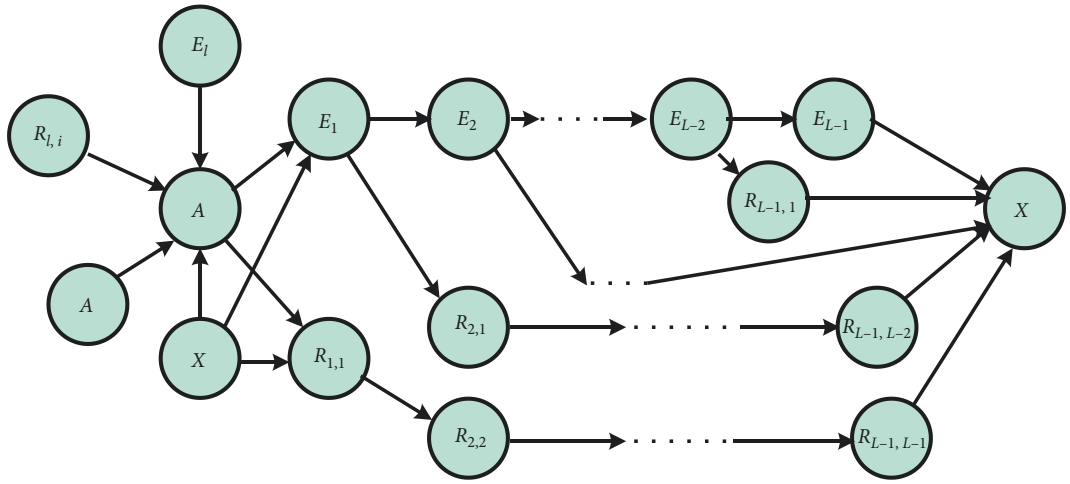


Figure 4: The DTMC model of ECS-HTCARQ protocol in an interference scenario.

Table 1: The states of the DTMC model.

| States | The meanings of the states |
|---|---|
| $A$ | The destination node $D$ successfully decodes the data frame |
| $X$ | When the maximum number of transmissions reaches $L$, the destination node $D$ does not successfully decode the data frame |
| $E_l$ | Neither the relay $R$ nor the destination node $D$ successfully decodes the data frame in the $l$th transmission |
| $R_{l,m}$ | In the $l$th transmission, the relay successfully decodes the data frame $m$ times, while the destination node $D$ does not successfully decode the data frame |

Using (20), we can solve for $\pi_1$, which can be expressed as

$$\pi_1 = \frac{1-\Pr_{AE_1}\Pr_{E_1^X}-\Pr_{AR_{1,1}}\Pr_{R_{1,1}^X}}{2-\Pr_{AA}} = \frac{1-\Pr(SR_{\text{out},1})\Pr(SD_{\text{out},2})-\Pr(\text{SRD}_{\text{out},2})(1-\Pr(SR_{\text{out},1}))}{1+\Pr(SD_{\text{out},1})}. \tag{21}$$

To find the steady-state probability $\pi_1^*$ when $L = 3$, the one-step transition probability matrix $P^*$ of the DTMC model is given as

$$P^* = \begin{pmatrix} \Pr_{AA} & 0 & \Pr_{AE_1} & 0 & \Pr_{AR_{1,1}} & 0 & 0 \\ \Pr_{XA} & 0 & \Pr_{XE_1} & 0 & \Pr_{XR_{1,1}} & 0 & 0 \\ \Pr_{E_1A} & 0 & 0 & \Pr_{E_1E_2} & 0 & \Pr_{E_1R_{2,1}} & 0 \\ \Pr_{E_2A} & \Pr_{E_2X} & 0 & 0 & 0 & 0 & 0 \\ \Pr_{R_{1,1}A} & 0 & 0 & 0 & 0 & 0 & \Pr_{R_{1,1}R_{2,2}} \\ \Pr_{R_{2,1}A} & \Pr_{R_{2,1}X} & 0 & 0 & 0 & 0 & 0 \\ \Pr_{R_{2,2}A} & \Pr_{R_{2,2}X} & 0 & 0 & 0 & 0 & 0 \end{pmatrix}. \tag{22}$$

Similarly, there is an equation

$$\begin{aligned} &\Big\{ \Pr_{AA}\pi_1^* + \Pr_{XA}\pi_2^* + \Pr_{E_1A}\pi_3^* + \Pr_{E_2A}\pi_4^* + \Pr_{R_{1,1}A}\pi_5^* \\ &+ \Pr_{R_{2,1}A}\pi_6^* + \Pr_{R_{2,2}A}\pi_7^* = \pi_1^*\Pr_{E_2X}\pi_4^* + \Pr_{R_{2,1}X}\pi_6^* + \Pr_{R_{2,2}X}\pi_7^* \\ &= \pi_2^*\Pr_{AE_1}\pi_1^* + \Pr_{XE_1}\pi_2^* = \pi_3^*\Pr_{E_1E_2}\pi_3^* \\ &= \pi_4^*\Pr_{AR_{1,1}}\pi_1^* + \Pr_{XR_{1,1}}\pi_2^* \\ &= \pi_5^*\Pr_{E_1R_{2,1}}\pi_3^* = \pi_6^*\Pr_{R_{1,1}R_{2,2}}\pi_5^* \\ &= \pi_7^*\pi_1^* + \pi_2^* + \pi_3^* + \pi_4^* + \pi_5^* + \pi_6^* \\ &\quad + \pi_7^* \\ &= 1, \end{aligned} \tag{23}$$

where $\pi_1^*$ can be computed as

$$\pi_1^* = \frac{Q}{H}, \tag{24}$$

where $Q$ and $H$ are expressed by the following equations:

$$\begin{aligned} Q = 1 &+ \Pr_{AE_1}\Pr_{E_1E_2}\Pr_{E_2A} - \Pr_{AE_1}\Pr_{E_1R_{2,1}} \\ &- \Pr_{AR_{1,1}}\Pr_{R_{1,1}R_{2,2}} - \Pr_{AE_1}\Pr_{E_1E_2} \\ &+ \Pr_{AE_1}\Pr_{E_1R_{2,1}}\Pr_{R_{2,2}A} + \Pr_{AR_{1,1}}\Pr_{R_{1,1}R_{2,2}}\Pr_{R_{2,1}A}, \end{aligned} \tag{25}$$

$$\begin{aligned} H = 1 &+ \Pr_{XE_1} + \Pr_{AR_{1,1}} + \Pr_{XE_1}\Pr_{E_1E_2} \\ &+ \Pr_{XE_1}\Pr_{E_1R_{2,1}} + \Pr_{AR_{1,1}}\Pr_{R_{1,1}R_{2,2}}. \end{aligned} \tag{26}$$

Adopting the one-step transition probabilities, respectively, reduces to

$$\begin{aligned}
Q &= 1 + \Pr_{AE_1}\Pr_{E_1E_2}\Pr_{E_2A} - \Pr_{AE_1}\Pr_{E_1R_{2,1}} \\
&\quad - \Pr_{AR_{1,1}}\Pr_{R_{1,1}R_{2,2}} - \Pr_{AE_1}\Pr_{E_1E_2} \\
&\quad + \Pr_{AE_1}\Pr_{E_1R_{2,1}}\Pr_{R_{2,1}A} + \Pr_{AR_{1,1}}\Pr_{R_{1,1}R_{2,2}}\Pr_{R_{2,2}A} \\
&= 1 + \Pr_{AE_1}\Pr_{E_1E_2}\left(1 - \Pr_{E_2X}\right) - \Pr_{AE_1}\Pr_{E_1R_{2,1}} \\
&\quad - \Pr_{AR_{1,1}}\Pr_{R_{1,1}R_{2,2}} - \Pr_{AE_1}\Pr_{E_1E_2} \\
&\quad + \Pr_{AE_1}\Pr_{E_1R_{2,1}}\left(1 - \Pr_{R_{2,1}X}\right) + \Pr_{AR_{1,1}}\Pr_{R_{1,1}R_{2,2}}\left(1 - \Pr_{R_{2,2}X}\right) \\
&= 1 - \Pr_{AE_1}\Pr_{E_1E_2}\Pr_{E_2X} - \Pr_{AE_1}\Pr_{E_1R_{2,1}}\Pr_{R_{2,1}X} \\
&\quad - \Pr_{AR_{1,1}}\Pr_{R_{1,1}R_{2,2}}\Pr_{R_{2,2}X} \\
&= 1 - \Pr\left(SR_{\text{out},2}\right)\Pr\left(SD_{\text{out},3}\right) \\
&\quad + \Pr\left(SR_{\text{out},2}\right)\Pr\left(SRD_{\text{out},3}\right) - \Pr\left(SRD_{\text{out},3}\right),
\end{aligned} \tag{27}$$

$$\begin{aligned}
H &= 1 + \Pr_{XE_1} + \Pr_{AR_{1,1}} + \Pr_{XE_1}\Pr_{E_1E_2} \\
&\quad + \Pr_{XE_1}\Pr_{E_1R_{2,1}} + \Pr_{AR_{1,1}}\Pr_{R_{1,1}R_{2,2}} \\
&= 1 + \Pr\left(SD_{\text{out},1}\right) + \Pr\left(SD_{\text{out},2}\right)\Pr\left(SR_{\text{out},1}\right) \\
&\quad + \Pr\left(SRD_{\text{out},2}\right) - \Pr\left(SR_{\text{out},1}\right)\Pr\left(SRD_{\text{out},2}\right).
\end{aligned} \tag{28}$$

Substituting (27) and (28) back into (24), we obtain the final expression for $\pi_1^*$:

$$\pi_1^* = \frac{1 - \Pr\left(SR_{\text{out},2}\right)\Pr\left(SD_{\text{out},3}\right) + \Pr\left(SR_{\text{out},2}\right)\Pr\left(SRD_{\text{out},3}\right) - \Pr\left(SRD_{\text{out},3}\right)}{1 + \Pr\left(SD_{\text{out},1}\right) + \Pr\left(SD_{\text{out},2}\right)\Pr\left(SR_{\text{out},1}\right) + \Pr\left(SRD_{\text{out},2}\right) - \Pr\left(SR_{\text{out},1}\right)\Pr\left(SRD_{\text{out},2}\right)}. \tag{29}$$

The data frames are transmitted within $(1-\alpha)T$. To simplify the calculation, let $T = 1$, and then the throughput of $L = 2$ and $L = 3$ can be expressed as follows, respectively:

$$\begin{aligned}
Th &= (1-\alpha)\frac{1 - \Pr\left(SR_{\text{out},1}\right)\Pr\left(SD_{\text{out},2}\right) - \Pr\left(SRD_{\text{out},2}\right)\left(1 - \Pr\left(SR_{\text{out},1}\right)\right)}{1 + \Pr\left(SD_{\text{out},1}\right)}, \\
Th^* &= (1-\alpha)\frac{1 - \Pr\left(SR_{\text{out},2}\right)\Pr\left(SD_{\text{out},3}\right) + \Pr\left(SR_{\text{out},2}\right)\Pr\left(SRD_{\text{out},3}\right) - \Pr\left(SRD_{\text{out},3}\right)}{1 + \Pr\left(SD_{\text{out},1}\right) + \Pr\left(SD_{\text{out},2}\right)\Pr\left(SR_{\text{out},1}\right) + \Pr\left(SRD_{\text{out},2}\right) - \Pr\left(SR_{\text{out},1}\right)\Pr\left(SRD_{\text{out},2}\right)}.
\end{aligned} \tag{30}$$

## 5. Numerical Results and Discussion

In this section, we present numerical results to analyze the impact of the system parameters on the end-to-end outage probability and throughput performance and compare the ECS-HTCARQ protocol and the Noncooperative automatic retransmission request (non-CARQ) protocol under this system model. The trade-off of the throughput and outage probability on the time allocation factor $\alpha$ is further investigated. Since this paper considers the destination node to use SC for data fusion and in many practical applications, the system performance at high SIR is of great importance and use [30]. Therefore, the basic parameters are set as follows: $\sigma_{SR}^2 = \sigma_{R\,D}^2 = 1$, $\sigma_{S\,D}^2 = 0.5$, $\sigma_{I_1R}^2 = \sigma_{I_2D}^2 = 0.1$, and $P_{I_1R} = P_{I_2D} = 5\ dB\ m$.

Figure 5 shows the variation of $\Pr(SRD_{\text{out},l})$ with $r_{th}\,(bit\,(1-\alpha)/Hz)$ under the parameter settings of $R_l = 1$, $L = 2$, 3, and $P_R = 20$dBm, 25dBm, 30dBm. It can be seen that the outage probability also tends to 0 when $r_{th}$ tends to 0, but as $r_{th}$ increases, the outage probability increases and reaches 1 in all cases. When $P_R$ is fixed, as $L$ increases, the outage probability decreases significantly; when $L$ is constant, as $P_R$ grows, the outage probability also improves obviously; when $L$ and $P_R$ increase simultaneously, the outage probability saturates to 1 and the $r_{th}$ value is extended, which is more suitable for high $r_{th}$ scenario. In addition, we compare the outage probability under the non-CARQ and find the CARQ technique can effectively reduce the outage probability. Because the redundant information of each retransmission improves the coding efficiency when the number of transmissions increases, which reduces the data frame transmission error rate. When the $P_R$ increases, the energy-constrained source node can collect more energy

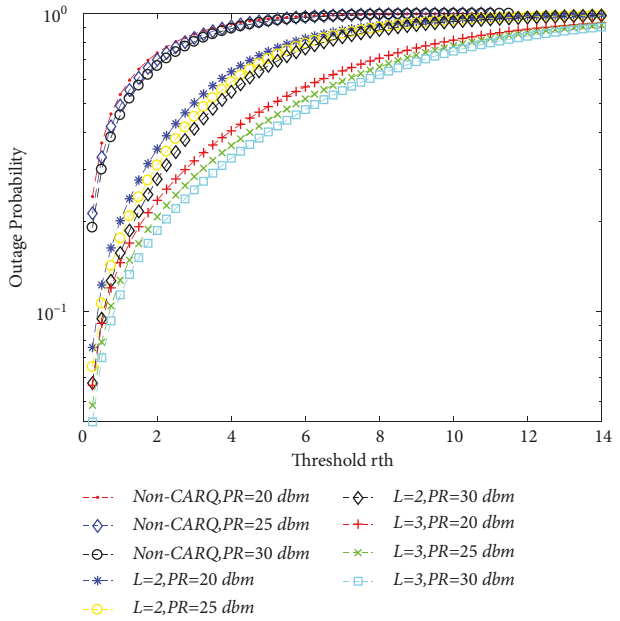


FIGURE 5: $r_{th}$ vs $\Pr(SRD_{\text{out},l})$ with different $L$ and $P_R$.

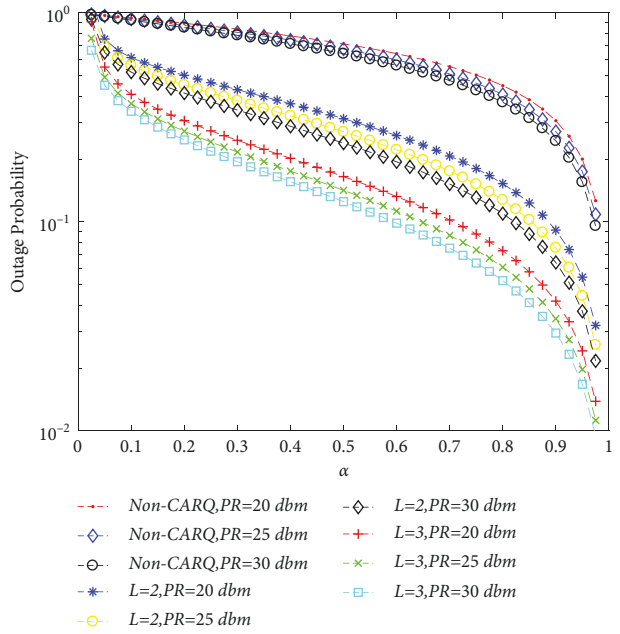


FIGURE 6: $\alpha$ vs $\Pr(SRD_{\text{out},l})$ with different $L$ and $P_R$.

through the RF signal, which will reduce the end-to-end outage probability.

In Figure 6, the variation of $\Pr(SRD_{\text{out},l})$ with $\alpha$ is compared for the parameter settings of $R_l = 1$, $L = 2$, 3, and $P_R$ = 20dBm, 25dBm, 30dBm. As $\alpha$ increases, the source node can obtain more energy to ensure data transmission, which will reduce the outage probability. When $\alpha$ goes from 0.1 to 0.8, it is observed that the outage probability decreases and becomes relatively saturated, the reason is that when $\alpha$ reaches a certain value, the source node has collected sufficient energy and ensured reliable data transmission. When $L$ and $P_R$ increase simultaneously, the ECS-HTCARQ protocol shows a significant reduction in outage performance compared to the non-CARQ protocol.

In Figure 7, we investigate the variation of $\Pr(SRD_{\text{out},l})$ with $\eta$ for the parameter settings of $R_l = 1$, $L = 2$, 3, and $P_R$ = 20dBm, 25dBm, 30dBm. When$\eta$ is higher, the improvement of outage performance is more significant. In practice, the outage probability is reduced by improving the intrinsic circuit structure of the network nodes to increase energy harvesting efficiency. As $L$ and $P_R$ increase simultaneously, there is a significant reduction in the outage probability.

In Figure 8, the variation of throughput with $\alpha$ is considered for the cases of non-CARQ, $L = 2$, $R_l = 1$, and $L = 3$, $R_l = 1$, 2. The numerical result finds the difference in throughput is small as $L$ increases, with an overall trend of increasing and then decreasing. When $\alpha$ tends to 0 or 1, based on the closed-form expression of throughput, the two curves both tend to 0 as well as conform to the rising and then falling trend of the image. Combined with Figure 6, there is a significant decrease in the outage probability with increasing $\alpha$, but the $\alpha$ value cannot be increased to 1. To maximize the system throughput, Figure 8 demonstrates there exists an optimal $\alpha$ for all cases. In addition, the

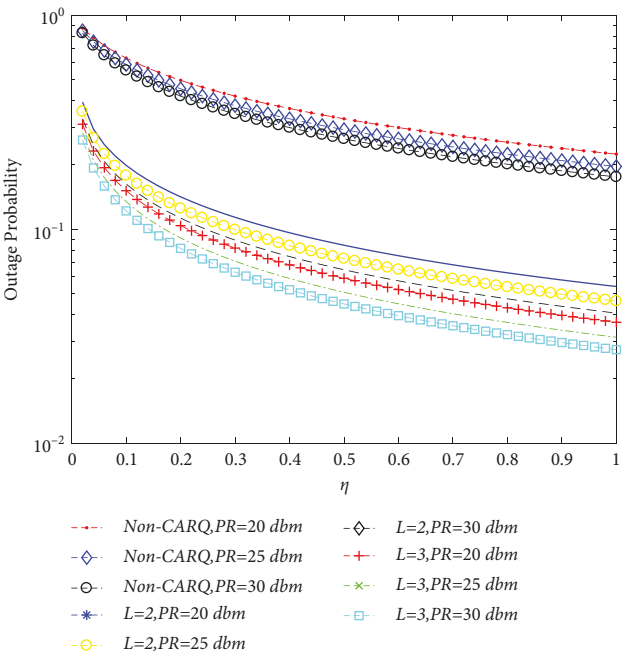


FIGURE 7: $\eta$ vs $\Pr(SRD_{\text{out},l})$ with different $L$ and $P_R$.

optimal $\alpha$ for the ECS-HTCARQ protocol is smaller than the non-CARQ protocol because only the redundant information is retransmitted each time, not the entire data frame. Although the difference in throughput is smaller as $L$ increases, there is a significant decrease in outage probability. Thus, we introduce the CARQ technology as effective.

Figure 9 compares the variation of throughput with $P_R$ for non-CARQ, $L = 2$, $R_l = 1$ and $L = 3$, $R_l = 1$, 2; it shows an overall increasing trend. When the $P_R$ increases to 30dBm, the ECS-HTCARQ protocol is superior to the non-CARQ protocol,

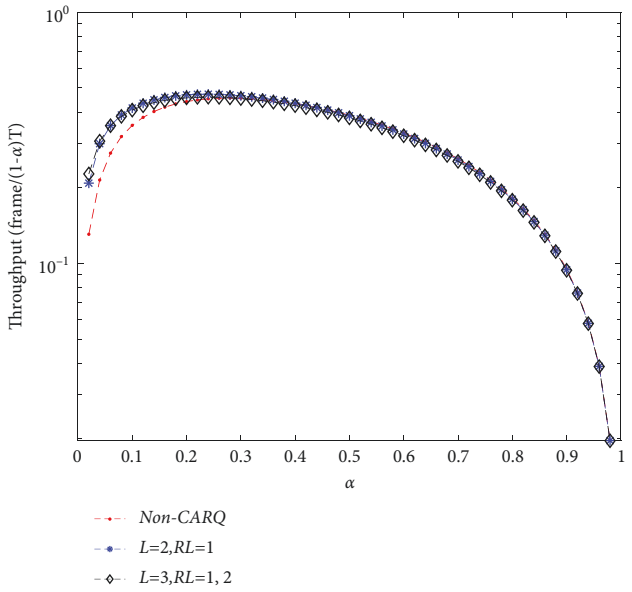


Figure 8: $\alpha$ vs throughput with different $L$.

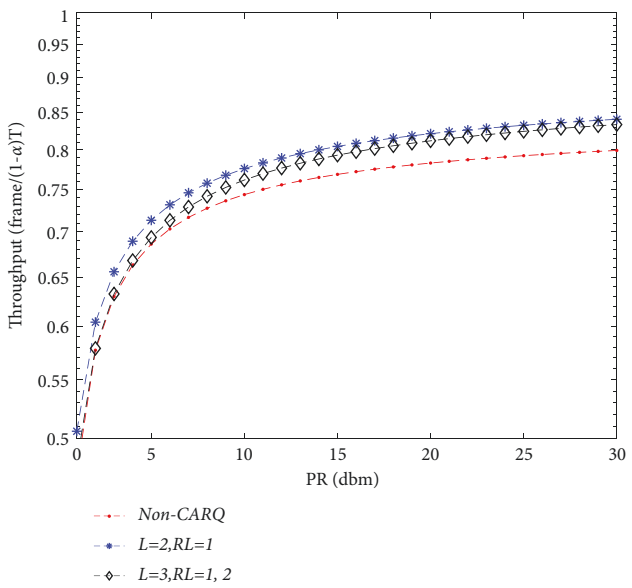


Figure 9: $P_R$ vs throughput with different $L$.

and the throughput curves tend to be the same for $L = 2$, $R_l = 1$ and $L = 3$, $R_l = 1, 2$. Combined with Figure 6, when $L$ and $P_R$ increase simultaneously, the two throughput curves converge but the outage probabilities decrease significantly.

According to Figures 6 and 8 and 10, further consider the optimal $\alpha$ versus $P_R$ for non-CARQ, $L = 2$, $R_l = 1$, $L = 3$, $R_l = 1$, and $L = 3$, $R_l = 2$. Note that the optimal $\alpha$ can easily be obtained by a one-dimension exhaustive search. It can be seen that the optimal $\alpha$ decreases when $L$ increases and the relay successfully decode early, and the optimal $\alpha$ is smaller such that there is more sufficient time for data transmission. When $P_R = 25$dBm, the optimal $\alpha$ values are 0.41, 0.3, 0.2, and 0.24 for the cases of the non-CARQ, $L = 2$, $R_l = 1$, $L = 3$, $R_l = 1$, and $L = 3$, $R_l = 2$, respectively.

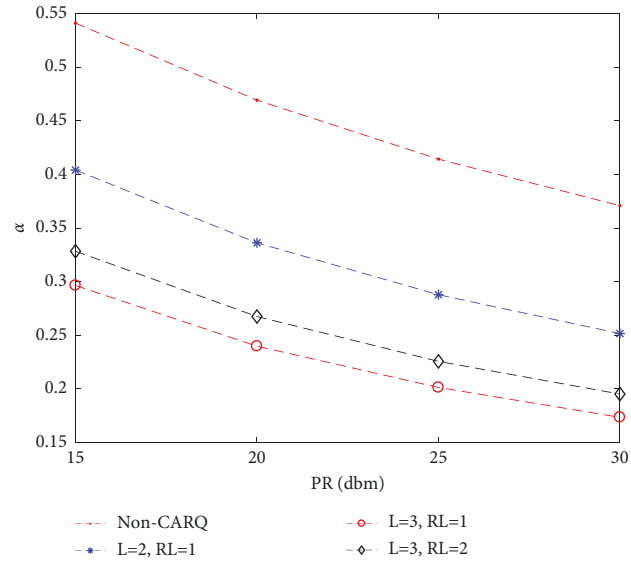


Figure 10: $P_R$ vs $\alpha$ with different $L$ and $R_l$.

## 6. Conclusion

In this paper, we propose the ECS-HTCARQ protocol in the interference scenario. The three-node model of WPCCN and data frame transmission mechanism are described, the DTMC model is established, and the closed-form expressions for the outage probability and the throughput are derived under Rayleigh fading channels. Numerical results show that the introduction of CARQ technology leads to smaller differences in throughput. However, with an increasing number of transmissions, a significant reduction in outage probability and CARQ technology further improves the reliability of the overall system data transmission. The optimal $\alpha$ for a specific $L$ and $P_R$ value is given. It is found when $L$ increases and the relay successfully decode early, the optimal $\alpha$ is smaller, which is beneficial to enhance the data frame transmission time. To further improve the system performance of the considered networks, future work will extend this model to the case of multiple relays to give the optimal relay selection scheme.

## Appendix

Before expanding the calculation, let $X = |h_{R,S}|^2$, $Y = |h_{S,R}|^2$, $Z = |h_{I_1,R}|^2$, $X_1 = |h_{S,D}|^2$, $Y_1 = |h_{R,D}|^2$, and $Z_1 = |h_{I_2,D}|^2$.

To compute the closed-form expression of equation (9), we give the following proposition.

**Proposition 1.** *When $X$ and $Y$ are the random variables and $C$ is a constant, $\Pr\{XY < C\}$, $\Pr\{X/Y < C\}$ can be calculated as*

$$\begin{aligned}\Pr\{XY < C\} &= \int_0^{+\infty} \Pr\left\{X < C\frac{1}{y} | Y = y\right\} f_Y(y)\mathrm{d}y \\ &= \int_0^{+\infty} F_X\left(\frac{C}{y}\right) f_Y(y)\mathrm{d}y,\end{aligned} \tag{A.1}$$

$$\Pr\left\{\frac{X}{Y}<C\right\}=\int_0^{+\infty}\Pr\{X<Cy|Y=y\}f_Y(y)\mathrm{d}y=\int_0^{+\infty}F_X(Cy)f_Y(y)\mathrm{d}y. \tag{A.2}$$

Equation (9) can be expanded as

$$\begin{aligned}\Pr\left(SR_{\mathrm{out},l}\right)&=\Pr\left\{l\log\left(1+\frac{\alpha/1-\alpha\eta P_R\left|h_{R,S}\right|^2\left|h_{S,R}\right|^2}{P_{I_1}\left|h_{I_1,R}\right|^2}\right)<r\right\}\\&=\Pr\left\{\frac{\alpha/1-\alpha\eta P_R\left|h_{R,S}\right|^2\left|h_{S,R}\right|^2}{P_{I_1}\left|h_{I_1,R}\right|^2}<2^{\frac{r}{l}}-1\right\}\\&=\Pr\left\{\frac{\left|h_{R,S}\right|^2\left|h_{S,R}\right|^2}{\left|h_{I_1,R}\right|^2}<\frac{2^{r/l}-1}{\mu}\right\}=\Pr\left\{\frac{XY}{Z}<\tau\right\}=\int_0^{+\infty}\Pr\{XY<\tau z\}f_Z(z)\mathrm{d}z\\&=\int_0^{+\infty}\int_0^{+\infty}\Pr\left\{X<\frac{\tau z}{y}\right\}f_Y(y)\mathrm{d}y f_Z(z)\mathrm{d}z\\&=\int_0^{+\infty}\int_0^{+\infty}F_X\left(\frac{\tau z}{y}\right)f_Y(y)\mathrm{d}y f_Z(z)\mathrm{d}z\\&=\int_0^{+\infty}\int_0^{+\infty}\left(\left(1-\exp\left(-\frac{1}{y}\frac{\tau z}{\sigma_{R,S}^2}\right)\right)\frac{1}{\sigma_{S,R}^2}\exp\left(-\frac{1}{\sigma_{S,R}^2}y\right)\right)\mathrm{d}y\frac{1}{\sigma_{I_1,R}^2}\exp\left(-\frac{1}{\sigma_{I_1,R}^2}z\right)\mathrm{d}z\\&=\int_0^{+\infty}\left(1-\frac{1}{\sigma_{S,R}^2}\int_0^{+\infty}\exp\left(-\frac{1}{y}\frac{\tau z}{\sigma_{R,S}^2}-\frac{1}{\sigma_{S,R}^2}y\right)\mathrm{d}y\right)\frac{1}{\sigma_{I_1,R}^2}\exp\left(-\frac{1}{\sigma_{I_1,R}^2}z\right)\mathrm{d}z\\&=\int_0^{+\infty}\left(1-\sqrt{\frac{4\tau z}{\sigma_{R,S}^2\sigma_{S,R}^2}}K_1\left(\sqrt{\frac{4\tau z}{\sigma_{R,S}^2\sigma_{S,R}^2}}\right)\right)\frac{1}{\sigma_{I_1,R}^2}\exp\left(-\frac{1}{\sigma_{I_1,R}^2}z\right)\mathrm{d}z\\&=1-\frac{1}{\sigma_{I_1,R}^2}\int_0^{+\infty}\sqrt{\frac{4\tau z}{\sigma_{R,S}^2\sigma_{S,R}^2}}K_1\left(\sqrt{\frac{4\tau z}{\sigma_{R,S}^2\sigma_{S,R}^2}}\right)\exp\left(-\frac{1}{\sigma_{I_1,R}^2}z\right)\mathrm{d}z,\end{aligned} \tag{A.3}$$

where $\int_0^{+\infty}x^{\nu-1}\exp(-\beta/x-\gamma x)\mathrm{d}x=2(\beta/\gamma)^{\nu/2}K_\nu(2\sqrt{\beta\gamma})$, $K_\nu(\bullet)$ is the $\nu$th order modified Bessel function of the second kind, $\mu=(\alpha/1-\alpha\eta P_R)/P_{I_1}$, and $\tau=2^{r/l}-1/\mu$.

To further derive the closed-form expression for equation (9), query the integral expressions for the product of the $\nu$th order modified Bessel function of the second kind, exponential, and power functions according to the literature [31], and from 6.631(3), we have

$$\begin{aligned}&\int_0^{+\infty}x^{\mu-(r/l)}\exp(-\alpha x)K_{2\nu}(2\beta\sqrt{x})\mathrm{d}x\\&=\frac{\Gamma(\mu+\nu+1/2)\Gamma(\mu-\nu+1/2)}{2\beta}\exp\left(\frac{\beta^2}{2\alpha}\right)\alpha^{-\mu}W_{-\mu,\nu}\left(\frac{\beta^2}{\alpha}\right),\end{aligned} \tag{A.4}$$

where $W_{-\mu,\nu}(\bullet)$ is the Whittaker function.

Substituting equation (A 4) into equation (A 3), we finally obtain the closed-form expression of equation (9) as

$$\begin{aligned}\Pr\left(SR_{\mathrm{out},l}\right)&=1-\frac{1}{\sigma_{I_1,R}^2}\int_0^{+\infty}\sqrt{\frac{4\tau z}{\sigma_{R,S}^2\sigma_{S,R}^2}}K_1\left(\sqrt{\frac{4\tau z}{\sigma_{R,S}^2\sigma_{S,R}^2}}\right)\exp\left(-\frac{1}{\sigma_{I_1,R}^2}z\right)\mathrm{d}z\\&=1-\frac{1}{\sigma_{I_1,R}^2}2\sqrt{\frac{\tau}{\sigma_{R,S}^2\sigma_{S,R}^2}}\frac{\Gamma(2)\Gamma(1)}{2\sqrt{\tau/\sigma_{R,S}^2\sigma_{S,R}^2}}\\&\quad\times\exp\left(\frac{\left(\tau\sigma_{I_1,R}^2/\sigma_{R,S}^2\sigma_{S,R}^2\right)}{2}\right)\sigma_{I_1,R}^2W_{-1,(1/2)}\left(\frac{\tau\sigma_{I_1,R}^2}{\sigma_{R,S}^2\sigma_{S,R}^2}\right)\\&=1-\exp\left(\frac{\left(\tau\sigma_{I_1,R}^2/\sigma_{R,S}^2\sigma_{S,R}^2\right)}{2}\right)W_{-1,(1/2)}\left(\frac{\tau\sigma_{I_1,R}^2}{\sigma_{R,S}^2\sigma_{S,R}^2}\right).\end{aligned} \tag{A.5}$$

Similarly, the closed-form expression of equation (10) is obtained as

$$\begin{aligned}
\Pr\left(SD_{\text{out},l}\right) &= \Pr\left\{ l\log\left(1+\frac{\alpha/1-\alpha\eta P_R\left|h_{R,S}\right|^2\left|h_{S,D}\right|^2}{P_{I_2}\left|h_{I_2,D}\right|^2}\right)<r\right\}\\
&= \Pr\left\{\frac{\left|h_{R,S}\right|^2\left|h_{S,D}\right|^2}{\left|h_{I_2,D}\right|^2}<\frac{2^{r/l}-1}{\mu_1}\right\}\\
&= \Pr\left\{\frac{XX_1}{Z_1}<\tau_1\right\}\\
&= 1-\frac{1}{\sigma_{I_2,D}^2}\int_0^{+\infty}\sqrt{\frac{4\tau_1 z_1}{\sigma_{R,S}^2\sigma_{S,D}^2}}K_1\left(\sqrt{\frac{4\tau_1 z_1}{\sigma_{R,S}^2\sigma_{S,D}^2}}\right)\exp\left(-\frac{1}{\sigma_{I_2,D}^2}z_1\right)\mathrm{d}z_1\\
&= 1-\exp\left(\frac{\tau_1\sigma_{I_2,D}^2}{2\sigma_{R,S}^2\sigma_{S,D}^2}\right)W_{-1,(1/2)}\left(\frac{\tau_1\sigma_{I_2,D}^2}{\sigma_{R,S}^2\sigma_{S,D}^2}\right),
\end{aligned} \tag{A.6}$$

where $\mu_1 = \alpha/1-\alpha\eta P_R/P_{I_2}$ and $\tau_1 = 2^{r/l}-1/\mu_1$.

The closed-form expression of equation (11) is

$$\begin{aligned}
\Pr\left(SRD_{\text{out},l}\right) &= \Pr\left\{ l\log\left(1+\frac{\alpha/1-\alpha\eta P_R\left|h_{R,S}\right|^2\left|h_{S,D}\right|^2}{P_{I_2}\left|h_{I_2,D}\right|^2}\right)<r,(l-R_l)\log\left(1+\frac{P_R\left|h_{R,D}\right|^2}{P_{I_2}\left|h_{I_2,D}\right|^2}\right)<r\right\}\\
&= \Pr\left\{\frac{\left|h_{R,S}\right|^2\left|h_{S,D}\right|^2}{\left|h_{I_2,D}\right|^2}<\frac{2^{r/l}-1}{\mu_1},\frac{\left|h_{R,D}\right|^2}{\left|h_{I_2,D}\right|^2}<\frac{2^{r/(l-R_l)}-1}{\mu_2}\right\}\\
&= \int_0^{+\infty}\Pr\left\{\left|h_{R,S}\right|^2\left|h_{S,D}\right|^2<\frac{2^{r/l}-1}{\mu_1}z_1,\left|h_{R,D}\right|^2<\frac{2^{r/(l-R_l)}-1}{\mu_2}z_1\right\}f_{Z_1}(z_1)\mathrm{d}z_1\\
&= \int_0^{+\infty}\Pr\left\{\left|h_{R,S}\right|^2\left|h_{S,D}\right|^2<\frac{2^{r/l}-1}{\mu_1}z_1\right\}\Pr\left\{\left|h_{R,D}\right|^2<\frac{2^{r/(l-R_l)}-1}{\mu_2}z_1\right\}f_{Z_1}(z_1)\mathrm{d}z_1\\
&= \int_0^{+\infty}\Pr\{XX_1<\tau_1 z_1\}\Pr\{Y_1<\tau_2 z_1\}f_{Z_1}(z_1)\mathrm{d}z_1\\
&= \int_0^{+\infty}\left[1-\sqrt{\frac{4\tau_1 z_1}{\sigma_{R,S}^2\sigma_{S,D}^2}}K_1\left(\sqrt{\frac{4\tau_1 z_1}{\sigma_{R,S}^2\sigma_{S,D}^2}}\right)\right]\left[1-\exp\left(-\frac{\tau_2 z_1}{\sigma_{R,D}^2}\right)\right]\frac{1}{\sigma_{I_2,D}^2}\exp\left(-\frac{z_1}{\sigma_{I_2,D}^2}\right)\mathrm{d}z_1\\
&= \int_0^{+\infty}\frac{1}{\sigma_{I_2,D}^2}\left[1-\sqrt{\frac{4\tau_1 z_1}{\sigma_{R,S}^2\sigma_{S,D}^2}}K_1\left(\sqrt{\frac{4\tau_1 z_1}{\sigma_{R,S}^2\sigma_{S,D}^2}}\right)\right]\left[\exp\left(-\frac{z_1}{\sigma_{I_2,D}^2}\right)-\exp\left(-\frac{\tau_2 z_1}{\sigma_{R,D}^2}-\frac{z_1}{\sigma_{I_2,D}^2}\right)\right]\mathrm{d}z_1\\
&= \int_0^{+\infty}\frac{1}{\sigma_{I_2,D}^2}\exp\left(-\frac{z_1}{\sigma_{I_2,D}^2}\right)\mathrm{d}z_1-\int_0^{+\infty}\frac{1}{\sigma_{I_2,D}^2}\exp\left(-\frac{z_1}{\sigma_{I_2,D}^2}\right)\sqrt{\frac{4\tau_1 z_1}{\sigma_{R,S}^2\sigma_{S,D}^2}}K_1\left(\sqrt{\frac{4\tau_1 z_1}{\sigma_{R,S}^2\sigma_{S,D}^2}}\right)\mathrm{d}z_1\\
&\quad-\int_0^{+\infty}\frac{1}{\sigma_{I_2,D}^2}\exp\left(-\frac{\tau_2 z_1}{\sigma_{R,D}^2}-\frac{z_1}{\sigma_{I_2,D}^2}\right)\mathrm{d}z_1\\
&\quad+\int_0^{+\infty}\frac{1}{\sigma_{I_2,D}^2}\sqrt{\frac{4\tau_1 z_1}{\sigma_{R,S}^2\sigma_{S,D}^2}}K_1\left(\sqrt{\frac{4\tau_1 z_1}{\sigma_{R,S}^2\sigma_{S,D}^2}}\right)\exp\left(-\frac{\tau_2 z_1}{\sigma_{R,D}^2}-\frac{z_1}{\sigma_{I_2,D}^2}\right)\mathrm{d}z_1\\
&= 1-\exp\left(\frac{\tau_1\sigma_{I_2,D}^2}{2\sigma_{R,S}^2\sigma_{S,D}^2}\right)W_{-1,(1/2)}\left(\frac{\tau_1\sigma_{I_2,D}^2}{\sigma_{R,S}^2\sigma_{S,D}^2}\right)-\frac{\sigma_{R,D}^2}{\tau_2\sigma_{I_2,D}^2+\sigma_{R,D}^2}+\exp\left(\frac{\left(\tau_1/\sigma_{R,S}^2\sigma_{S,D}^2\right)\sigma_{I_2,D}^2\sigma_{R,D}^2}{2\left(\tau_2\sigma_{I_2,D}^2+\sigma_{R,D}^2\right)}\right)\\
&\quad\times\frac{\sigma_{R,D}^2}{\tau_2\sigma_{I_2,D}^2+\sigma_{R,D}^2}W_{-1,(1/2)}\left(\frac{\left(\tau_1/\sigma_{R,S}^2\sigma_{S,D}^2\right)\sigma_{I_2,D}^2\sigma_{R,D}^2}{\tau_2\sigma_{I_2,D}^2+\sigma_{R,D}^2}\right),
\end{aligned} \tag{A.7}$$

where $\mu_2 = P_R/P_{I_2}$ and $\tau_2 = 2^{r/(l-R_l)} - 1/\mu_2$.

The closed-form expression of equation (12) is

$$\begin{aligned}\Pr\left(RD_{\text{out},l}\right) &= \Pr\left\{(l-R_l)\log\left(1+\frac{p_R\left|h_{R,D}\right|^2}{P_{I_2}\left|h_{I_2,D}\right|^2}\right)<r\right\}\\ &= \Pr\left\{\frac{\left|h_{R,D}\right|^2}{\left|h_{I_2,D}\right|^2}<\frac{2^{r/(l-R_l)}-1}{\mu_2}\right\}\\ &= \int_0^{+\infty}\Pr\{Y_1<\tau_2 z_1\}f_{Z_1}(z_1)\mathrm{d}z_1\\ &= \int_0^{+\infty}\left[1-\exp\left(-\frac{\tau_2 z_1}{\sigma_{R,D}^2}\right)\right]\frac{1}{\sigma_{I_2,D}^2}\exp\left(-\frac{z_1}{\sigma_{I_2,D}^2}\right)\mathrm{d}z_1\\ &= 1-\frac{\sigma_{R,D}^2}{\tau_2\sigma_{I_2,D}^2+\sigma_{R,D}^2}.\end{aligned} \tag{A.8}$$

## Data Availability

The data used to support the findings of this study are from previously reported studies and datasets, which have been cited.

## Conflicts of Interest

The authors declare that they have no conflicts of interest.

## Acknowledgments

This work was supported by the Gansu Provincial Department of Education, Innovation Fund Project (2022A-019), the National Natural Science Foundation of China (61663024), the Ph.D. Research Startup Fund of Lanzhou University of Technology (05-061405), and the Hongliu Fund of First-class Disciplines of Lanzhou University of Technology, China.

## References

[1] H. Chen, C. Zhai, Y. H. Li, and B. Vucetic, "Cooperative strategies for wireless-powered communications: an Overview," *IEEE Wireless Communications*, vol. 25, no. 4, pp. 112–119, 2018.

[2] P. D. Nguyen and L. W. Kim, "Sensor system: a Survey of sensor Type, Ad Hoc network Topology and energy harvesting techniques," *Electronics*, vol. 10, no. 2, p. 219, 2021.

[3] V. N. Vo, H. Tran, V. L. Dao, C. So-In, D. D. Tran, and E Uhlemann, "On communication performance in energy harvesting WSNs under a cooperative Jamming Attack," *IEEE Systems Journal*, vol. 14, no. 4, pp. 4955–4966, 2020.

[4] D. B. Jiao, P. Yang, L. Q. Fu, L. Ke, and K. Tang, "Optimal energy-delay scheduling for energy-harvesting WSNs with interference channel via negatively Correlated Search," *IEEE Internet of Things Journal*, vol. 7, no. 3, pp. 1690–1703, 2020.

[5] R. R. Zhang, J. Yu, Y. Guan, and J. Liu, "A Dominating set-based sleep scheduling in energy harvesting WBANs," *IEEE Transactions on Vehicular Technology*, vol. 70, no. 11, pp. 11923–11934, 2021.

[6] J. Baek, S. I. Han, and Y. Han, "Optimal UAV Route in wireless charging sensor networks," *IEEE Internet of Things Journal*, vol. 7, no. 2, pp. 1327–1335, 2020.

[7] R. Zhang and C. K. Ho, "MIMO broadcasting for simultaneous wireless information and power transfer," *IEEE Transactions on Wireless Communications*, vol. 12, no. 5, pp. 1989–2001, 2013.

[8] X. Zhou, R. Zhang, and C. K. Ho, "Wireless information and power transfer: architecture Design and rate-energy Tradeoff," *IEEE Transactions on Communications*, vol. 61, no. 11, pp. 4754–4767, 2013.

[9] H. Chen, Y. X. Jiang, Y. H. Li, Y. Ma, and B. Vucetic, "A Game-Theoretical Model for Wireless Information and Power Transfer in Relay Interference Channels," in *Proceedings of the 2014 IEEE International Symposium on Information Theory*, pp. 1161–1165, IEEE, Honolulu, HI, USA, June 2014.

[10] P. Grover and A. Sahai, "Shannon Meets Tesla: Wireless Information and Power Transfer," in *Proceedings of the 2010 IEEE International Symposium on Information Theory*, pp. 2363–2367, IEEE, Austin, TX, USA, June 2010.

[11] Q. Li and D. Xu, "Outage Minimized Joint Power Splitting and Resource Allocation Optimization for Multiuser OFDM Systems with SWIPT," in *Proceedings of the 2019 IEEE/CIC International Conference on Communications in China*, August 2019.

[12] S. H. Kim and D. I. Kim, "Hybrid Backscatter Communication for Wireless Powered Communication Networks," in *Proceedings of the 2016 13th International Symposium on Wireless Communication Systems*, pp. 265–269, IEEE, Poznan, Poland, September 2016.

[13] B. Lyu, H. Y. Guo, Z. Yang, and G. Gui, "Throughput maximization for hybrid backscatter assisted cognitive wireless powered radio networks," *IEEE Internet of Things Journal*, vol. 5, no. 3, pp. 2015–2024, 2018.

[14] F. Yang, W. J. Xu, Z. Zhang, L. Guo, and J. Lin, "Energy efficiency maximization for relay-assisted WPCN: joint time duration and power allocation," *IEEE Access*, vol. 6, pp. 78297–78307, 2018.

[15] B. E. Y. Belmekki, A. Hamza, and B. Escrig, "Performance analysis of cooperative communications at road intersections using stochastic geometry tools," *Digital Signal Processing*, vol. 116, no. 2021, Article ID 103112, 2021.

[16] X. N. Tran, V. P. Hoang, and B. C. Nguyen, "Combining RF energy harvesting and cooperative communications for low-power wide-area systems," *AEU-International Journal of Electronics and Communications*, vol. 139, no. 2021, Article ID 153909, 2021.

[17] N. BenHalima and H. Boujemaa, "Cooperative communications with optimal harvesting duration for Nakagamifading channels," *Turkish Journal of Electrical Engineering and Computer Sciences*, vol. 28, no. 2, pp. 621–634, 2020.

[18] X. H. Shang, H. Yin, Y. D. Wang, M. Li, and Y. Wang, "Secure Multiuser scheduling for hybrid relay-assisted wireless powered cooperative communication networks with Full-duplex destination-based Jamming," *IEEE Access*, vol. 9, pp. 49774–49787, 2021.

[19] L. S. Cerqueira, A. B. Vieira, L. F. M. Vieira, M. A. M. Vieira, and J. A. M. Nacif, "A cooperative protocol for pervasive underwater acoustic networks," *Wireless Networks*, vol. 27, no. 3, pp. 1941–1963, 2021.

[20] X. W. Li, J. J. Li, Y. Liu, Z. Ding, and A. Nallanathan, "Residual Transceiver Hardware Impairments on cooperative NOMA

networks," *IEEE Transactions on Wireless Communications*, vol. 19, no. 1, pp. 680–695, 2020.

[21] X. S. Liang, S. Jin, W. J. Wang, X. Gao, and K. K. Wong, "Outage probability of amplify-and-forward two-Way relay interference-limited systems," *IEEE Transactions on Vehicular Technology*, vol. 61, no. 7, pp. 3038–3049, 2012.

[22] T. N. Do and B. An, "Cooperative spectrum sensing schemes with the interference Constraint in cognitive radio networks," *Sensors*, vol. 14, no. 5, pp. 8037–8056, 2014.

[23] S. Lee, W. F. Su, S. Batalama, and J. D. Matyjas, "Cooperative decode-and-forward ARQ relaying: performance analysis and power optimization," *IEEE Transactions on Wireless Communications*, vol. 9, no. 8, pp. 2632–2642, 2010.

[24] M. Tacca, P. Monti, and A. Fumagalli, "Cooperative and reliable ARQ protocols for energy harvesting wireless sensor nodes," *IEEE Transactions on Wireless Communications*, vol. 6, no. 7, pp. 2519–2529, 2007.

[25] H. L. Chen, Y. M. Cai, W. W. Yang, D. Zhang, and Y. Hu, "Throughput and energy efficiency of a novel cooperative ARQ strategy for wireless sensor networks," *Computer Communications*, vol. 35, no. 9, pp. 1064–1073, 2012.

[26] Y. Q. Zhou, B. Wang, L. Dai, and S. Li, "Performance analysis of Single source and multiple destinations cooperative GBn-ARQ over underwater wireless sensor networks," *Ad Hoc & Sensor Wireless Networks*, vol. 50, no. 1-4, pp. 55–71, 2021.

[27] A. Bletsas, A. G. Dimitriou, and J. N. Sahalos, "Interference-limited opportunistic relaying with reactive sensing," *IEEE Transactions on Wireless Communications*, vol. 9, no. 1, pp. 14–20, 2010.

[28] T. Soithong, V. A. Aalo, G. P. Efthymoglou, and C. Chayawan, "Performance of Multihop relay systems with Co-channel interference in Rayleigh fading channels," *IEEE Communications Letters*, vol. 15, no. 8, pp. 836–838, 2011.

[29] F. K. Ojo and M. F. Mohd Salleh, "Energy efficiency optimization for SWIPT-enabled cooperative relay networks in the presence of interfering transmitter," *IEEE Communications Letters*, vol. 23, no. 10, pp. 1806–1810, 2019.

[30] H. Chen, Y. H. Li, J. Luiz Rebelatto, B. F. Uchoa-Filho, and B. Vucetic, "Harvest-then-cooperate: wireless-powered cooperative communications," *IEEE Transactions on Signal Processing*, vol. 63, no. 7, pp. 1700–1711, 2015.

[31] I. S. G. Ryzhik and I. M. Ryzhik, *Table of Integrals, Series, and Products*, Elsevier, New York, NY, USA, 2007.